

Cold spray-based rapid and scalable production of printed flexible electronics

Semih Akin ^a, Seungjun Lee ^{a,b}, Seunghwan Jo ^a, Duygu Gazioglu Ruzgar ^{a,c}, Karthick Subramaniam ^{a,d}, Jung-Ting Tsai ^e, Martin Byung-Guk Jun ^{a,f,*}

^a School of Mechanical Engineering, Purdue University, West Lafayette, IN 47907, USA

^b School of Mechanical Engineering Technology, Kyungpook National University, Buk-gu Daegu 41566, South Korea

^c Metallurgical and Materials Engineering, Bursa Technical University, Bursa 16310, Turkey

^d Mechatronics and Instrumentation Lab, Department of Mechanical Engineering, Indian Institute of Technology Indore, Madhya Pradesh 453552, India

^e School of Materials Engineering, Purdue University, West Lafayette, IN 47907, USA

^f Indiana Manufacturing Competitiveness Center (IN-MaC), Purdue University, West Lafayette, IN 47907, USA

ARTICLE INFO

Keywords:

Additive manufacturing
Cold spray
Printed electronics
Flexible electronics
Direct writing
Sustainable repairing
Laser machining

ABSTRACT

Flexible electronics (FE) is attracting great attention from both scientific and industrial communities, and plays a crucial role in smart device applications. Despite great promise, traditional printing approaches (*e.g.*, screen printing, ink-jet printing, *etc.*) often need a high-temperature post-sintering process to produce FE with desired electrical conductivity and adhesion strength. The post-sintering processes, however, often lead to fast oxidation of the functional coating while limiting the use of low-thermal budget substrates. Exponential advance of FE in a large-scale and energy-efficient manner relies on rationally eliminating the post-sintering processes. To this end, with the aim of uncovering process-structure-properties relationships, we employ the emerging cold spray (CS) technique for rapid and scalable production of FE without a need for high-temperature post-sintering. In this regard, micron-scale Tin (Sn) particles are directly written on a flexible polymer substrate (PET) by cold spraying under ambient conditions. The effect of CS process parameters on the resultant coatings is comprehensively characterized in terms of microstructure, film thickness, electrical conductivity, linewidth, and adhesion strength. The resulting electrodes show excellent electrical conductivity ($6.98 \times 10^5 \text{ S m}^{-1}$), adhesion strength, long-term stability, and flexibility without significant conductivity loss after 1000 bending cycles. By leveraging the CS operational settings, a resistive macro-heater ($12 \times 15 \text{ cm}^2$) and an LED circuit ($2.5 \text{ cm} \times 18 \text{ cm}$) are fabricated to demonstrate the applicability of the CS in printed FE. Moreover, to address the low-spatial resolution of CS writing, a case study on sequential CS and femtosecond laser machining is performed, which further led to ultra-high resolution (*i.e.*, $30 \mu\text{m}$ linewidth) custom-designed flexible electrodes. Thus, the present study reveals the immense potential of the CS technique for rapid and scalable production of FE without the need for post-sintering.

1. Introduction

Flexible electronics (FE) are attracting great attention in both industry and academia, offering large-scale, low-cost, and smart devices on various substrates [1–5]. In particular, revolutionary changes in the internet of things (IoT), Industry 4.0, and wearable electronics

synergistically shift the paradigm from rigid to flexible electronics [6–9], leading to an increasing demand for low-cost, high-throughput, and energy-efficient manufacturing approaches for FE. In general, FE is produced using additive manufacturing (AM) methods mainly based on thin-film printing technologies to deposit the functional coating materials (*i.e.*, typically nanomaterial inks containing nanoparticles, nanowires, or nanotubes [1]) on surfaces in various designs without a need

Abbreviations: AM, Additive manufacturing; CS, Cold spray; Cu, Copper; DE, Deposition efficiency; EDX, Energy-dispersive X-ray spectroscopy; FE, Flexible electronics; IR, Infrared; NS, Nozzle speed; OM, Optical microscope; PET, Polyethylene terephthalate; PEN, Polyethylene naphthalate; SD, Spray distance; SEM, Scanning electron microscope; Sn, Tin; Zn, Zinc.

* Corresponding author at: School of Mechanical Engineering, Purdue University, West Lafayette, IN 47907, USA.

E-mail addresses: sakin@purdue.edu (S. Akin), lee4153@purdue.edu (S. Lee), jo30@purdue.edu (S. Jo), dgaziogl@purdue.edu (D.G. Ruzgar), subram94@purdue.edu (K. Subramaniam), tsai92@purdue.edu (J.-T. Tsai), mbgjun@purdue.edu (M.B.-G. Jun).

<https://doi.org/10.1016/j.addma.2022.103244>

Received 9 February 2022; Received in revised form 12 October 2022; Accepted 19 October 2022

Available online 2 November 2022

2214-8604/© 2022 Elsevier B.V. All rights reserved.

Nomenclature

A	Area
L	Length
N	Number of spray pass
P	Pressure
R	Resistance
R/R_0	Relative resistance
S	Siemens
T	Temperature
T_g	Glass transition temperature
t	Thickness
w	width
σ	Conductivity
v	Specific volume
ρ	Resistivity
Ω	Ohm

for etching and masking [3,10]. AM enables low-cost rapid prototyping of FE with desired features by minimizing the increasing number of electronic waste [3,11].

Current AM approaches in producing FE involve the use of either inkjet printing, screen printing, gravure printing, blade coating, aerosol jet printing, dip-pen lithography [12], or hybrid printing methods [13–18]. These methods transfer the functional inks (e.g., nanomaterial suspension or colloids) on flexible substrates either by physical contact (e.g., screen, gravure, blade printing) or non-contact (e.g., inkjet, aerosol jet printing) [19]. Despite great promise, these methods often require a high-temperature post-sintering process to increase the electrical conductivity and mechanical adhesion of the resultant functional coatings, thereby limiting the use of important low thermal-budget substrates such as polyethylene terephthalate (PET) and polyethylene naphthalate (PEN) [1,3]. In addition, post-sintering of metal inks leads to undesirable fast oxidation/corrosion of the resultant coating film [1]. As such, the exponential advance of printed FE relies on rationally eliminating or replacing the post-sintering processes with such methods that enable direct writing of functional materials on the target surface.

Herein, supersonic cold spraying, which is an emerging solid-state material consolidation technique, can be a promising candidate to

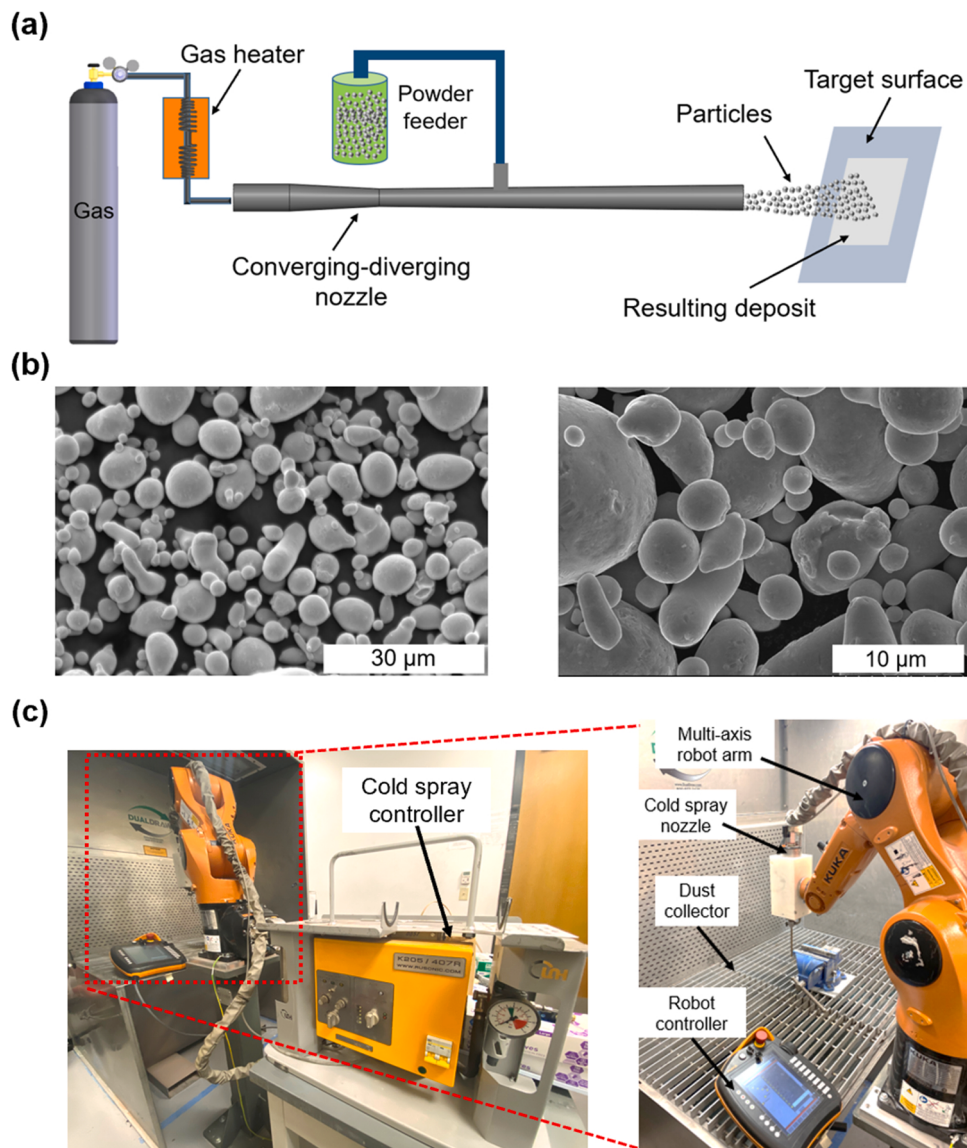


Fig. 1. (a) Schematic of a typical low-pressure cold spray setup and process, (b) Morphology of the feedstock Tin (Sn) particles at lower magnification (left panel) and higher magnification (right panel), (c) representative images of the cold spray experimental setup.

address the limitations of current printing approaches owing to its inherent advantages, including low-operating temperature, high deposition rate, high adhesion strength, and scalability [20–22]. As illustrated in Fig. 1a, a typical cold spray (CS) setup consists of a compressed gas supply, a supersonic nozzle (*i.e.*, converging-diverging nozzle), feedstock material (*i.e.*, typically micron-scale metal powders such as copper, aluminum, tin, zinc, steel, etc.), and a powder feeder. Traditionally, in the CS process, micron-scale (5–50 μm) feedstock metal powders are accelerated to supersonic velocities (*i.e.*, 300–1200 m/s) through a converging-diverging nozzle using compressed gases (*e.g.*, air, nitrogen, helium) followed by the impact onto a target substrate (*e.g.*, polymer, metal, ceramic, composite) [23–26]. Upon particles' impact on the target exceeding a critical impact velocity, the particles undergo plastic deformation (bonding), resulting in a dense and high-adhesion strength coating [24,27–30]. The unique advantages of the CS technique are its “low-operating temperature” and “high-adhesion strength”, which are highly-desired printing features in FE. In particular, the processing temperature of CS is always below the melting point of the feedstock particles, thereby “cold spray” is an oxidation-free process with a low risk of thermal degradation, and grain growth [31,32]. In addition, high-speed impingement of the feedstock materials facilitates the self-bonding of the particles onto the target surface, which leads to strong adhesion strength coating due to the particles' kinetic energy dispersion over the substrate surface [29]. As such, CS can be a promising candidate for rapid printing of functional materials on low-thermal budget substrates such as PET in a manner that high-performance FE could be rapidly produced without a need of post-sintering.

However, to the best knowledge of the authors, only a few studies have been reported on “solid-state” CS deposition of metal particles on polymer surfaces for FE [33,34]. Lee et al. [33] cold sprayed microscale copper ($D_{50} = 6 \mu\text{m}$) and nickel ($D_{50} = 1.64 \mu\text{m}$) powder mixture on the flexible PET surface at an inlet gas pressure (P) of 0.4 MPa and gas temperature (T) of 450–650°C with the spray pass number (N) of 15–20. Bhattacharya et al. [34] designed a micro cold spray device for the deposition of metal patterns on various substrates (*e.g.*, polyimide, PEEK, glass, etc.) for printed electronics, and they investigated the spraying compatibility between coating material and substrate under the spraying conditions of $P = 0.55 \text{ MPa}$ and $T = 250^\circ\text{C}$ [34]. Seongpil et al. [29] modified the downstream injection of the traditional CS nozzles to spray the “liquid-state” nanomaterial suspensions (*e.g.*, silver nanowires, copper nanoparticles) from atomized droplets, and applied this approach to produce FE such as photocathodes, wearable soft sensors, and supercapacitor electrodes at CS operational settings of $P = 0.2\text{--}0.4 \text{ MPa}$, $T = 200\text{--}450^\circ\text{C}$, and $N = 10\text{--}25$ passes [35–37]. Despite significant outputs, deployment of CS in FE remains challenging due to a lack of literature that comprehensively uncovers the process-structure-property relationships of the CS deposition process for printed FE. Moreover, in cold spraying, it is essential to achieve high-performance FE at low-gas temperatures (*e.g.*, room temperature) with a single-spray pass to compete with other commercially available printing technologies.

In this study, we aim to fill this gap by thoroughly investigating emerging solid-state CS particle deposition technology for printed FE. In this regard, micron-scale Tin (Sn) particles are directly cold sprayed onto the flexible PET surface at room temperature under vacuum-and mask-free conditions without a need for post-sintering process. Resultant coating properties are comprehensively studied in terms of microstructure, electrical resistance, film thickness, linewidth, surface roughness, and adhesion strength. The key research contributions of the present study are: 1) for the first time, CS deposition of micron-scale Sn particles on PET polymer surface at low temperatures is systematically studied for printed FE; 2) process-structure-property relationships of CS for FE is elucidated; 3) with an aim toward industrial applications, a millimeter-scale bendable resistive heater and an LED circuit are constructed as the FE applications to demonstrate the viability of CS in device fabrication; 4) potential of CS in sustainable repairing of

damaged FE is discussed in terms of ever-increasing number of electronic waste; 5) compatibility of CS with the fabrication of multi-material coatings is evaluated; 6) performance of CS with its pros and cons is analyzed against traditional printing methods; 7) a case study on sequential CS and femtosecond laser machining (cutting) is performed to address the low-spatial resolution of CS; 8) high-resolution (*i.e.*, 30 μm linewidth) custom-designed flexible electrodes with ultra-fine features are achieved through the proposed sequential CS and laser machining approach to show the scalability of CS in flexible electronics.

2. Materials and methods

2.1. Materials

Commercial micron-scale feedstock Tin (Sn) particles (Centerline-SST Inc., Catalog No: SST-S6001) were used as received without any further treatment. As shown in Fig. 1b, the morphology of the particles is in quasi-spherical shape, having a size distribution of 10–45 μm where the average diameter (d_{50}) is 17 μm [38]. Sn was selected as the coating material owing to its intrinsic physical and chemical properties of: (i) high corrosion resistance [39,40]; (ii) low melting temperature (232 °C) [41]; and (iii) soft nature ($\approx 7 \pm 1 \text{ HV}$ [42]) to facilitate the self-bonding onto the target polymer surface. Although copper (Cu) can be also considered as the feedstock candidate for FE due to its higher electrical conductivity as compared to Sn, achieving electrical conductivity by cold spraying of Cu on thermoplastics such as PET remains challenging due to the material jetting phenomenon [43]. In detail, the impingement of relatively hard particles (*e.g.*, Cu ($68 \pm 7 \text{ HV}$) [42]) onto a soft polymer substrate (*e.g.*, PET) leads to localized melting (*i.e.*, polymer jetting) on the polymer surface without achieving self-bonding of Cu particles (see Fig. S1a-c, *Supporting Information*). The polymer jetting and poor-bonding phenomena further act as a separator among the particles (Figs. S1b-c, *Supporting Information*), which prevents continuous electrical conductivity. The authors also observed that phenomenon in Refs [44,45], in which irregular-shaped Cu particles are cold sprayed onto the rigid ABS and Nylon 6 (polyamide) substrates, resulting in no electrically conductive coating by solely CS.

On the one hand, silver (Ag) is widely used as the functional ink in FE owing to its superior electrical conductivity and corrosion resistance with less reactivity as compared to Cu and Sn [1]. These functional Ag inks, however, are in a suspension form of either silver nanoparticles (AgNPs) or silver nanowires (AgNWs), thereby it is not applicable for traditional “solid-state” cold spraying applications. Although there are commercially available solid-state Ag powders in various sizes, the high cost of these powders (*i.e.*, 50 g of Ag powder in a size range of 2–3.5 μm = \$261 [46]) limits their pragmatic use in CS applications. Taken together, in the present study, we selected the Sn particles as the appropriate feedstock material for direct writing of FE at low temperatures without a need of high-temperature post-sintering.

As for the substrate material, polyethylene terephthalate (PET) sheet having a thickness of 0.25 mm (McMaster-Carr) was used as the flexible substrate owing to its common use in printed electronics, and inherent advantages including low-cost, low surface-roughness, recyclability, and optical transparency [4]. Despite its advantages, PET has a significantly low glass-transition temperature (T_g) (*i.e.*, 80 °C) [4], which limits the post-sintering of this important substrate to increase the electrical conductivity and mechanical adhesion strength. Moreover, repairing the damaged printings (electrodes) on the PET by the conventional soldering (*e.g.*, iron-lead soldering) methods remains challenging due to the low-thermal budget of PET polymer. Alternatively, employing the CS technique at low-processing temperatures (< 80°C) using soft and low-melting temperature feedstock materials such as Sn could address these problems without significantly compromising the intrinsic substrate (PET) and printing properties. In this regard, to uncover process-structure-property relationships with an aim toward industrial applications, the following sections are devoted to studying the CS

technique for rapid and scalable production of printed FE.

2.2. Experimental setup and methodology

A low-pressure cold spray machine (Rus Sonic Inc., Model no: K205/407 R) was employed in particle deposition experiments using the axisymmetric (circular-shaped) nozzle configuration with the dimensions of: convergent length= 10 mm; throat diameter = 2.54 mm; divergent length= 130 mm; and outlet diameter= 4.5 mm. The CS nozzle was mounted on a programmable multi-axis robot arm (Kuka KR Agilus) enclosed with a dust collector to precisely control the particle deposition process. The CS experimental setup is presented in Fig. 1c. The effect of CS operating parameters on important coatings properties (*i.e.*, electrical conductivity, coating thickness, linewidth, adhesion performance) was carefully investigated. The CS parameters and associated information used in this study are listed in Table 1. Air was used as the driving (propellant) gas. Sn particles were fed into the downstream of the nozzle at a feed rate of \approx 12 g/min, and CS experiments were conducted at room temperature under vacuum-and mask-free conditions. For each characterization, five-set of cold spray-coated specimens were prepared to average the outputs and calculate the standard deviations.

The electrical resistance of the resultant coatings was measured by the two-point probe method using a multimeter (Agilent/HP 34401A). The coating film thickness was measured by a digital micrometer (REXBETI) having a resolution of 1 μ m. The microstructure analysis of the surface and cross-sectional morphology of the coatings was conducted by optical microscopy (OM) and scanning electron microscopy (SEM) equipped with an X-ray (EDX) detector (Hitachi S-4800). For the cross-section SEM analysis, the samples were cut with an ultra-thin and extremely sharp razor blade followed by platinum sputtering to avoid the over-charging effects during the SEM characterization. The surface roughness of the coatings was characterized by a surface roughness tester (AMTAST). Both cross-cut and Scotch tape adhesion tests based on the ASTM D3359 standard were conducted to evaluate the adhesion properties of the as-cold sprayed Sn layers. The performance characterization of the fabricated flexible macro-heater was carried out using an infrared (IR) camera (FLIR A300). The surface of the specimens was cleaned with ethanol before and after the CS experiments to prevent possible contamination. All characterization studies were conducted at room temperature.

3. Results and discussion

This section discusses the effect of cold spray operating parameters (*i.e.*, gas pressure, nozzle speed, spray distance, and number of the spray pass) on resultant coatings in terms of electrical conductivity, film thickness, linewidth, surface roughness, and adhesion strength. Next, various FE circuits are fabricated to demonstrate the versatility of CS in printed FE. Lastly, a case study on sequential CS and ultra-fast laser machining is conducted to address the low-spatial resolution issue of CS.

3.1. Effect of gas pressure on resultant coating

Fig. 2a shows the effect of driving gas inlet pressure (P) on particles'

Table 1
Cold spray process parameters involved in the experiments.

Driving gas	Air
Driving gas pressure (MPa)	0.4, 0.5, 0.6, 0.7
Driving gas temperature (°C)	25
Powder feed rate (g/min)	\approx 12
Nozzle transverse speed (mm/s)	20, 30, 40, 50, 75, 100, 150
Spray distance (stand-off distance) (mm)	10, 20, 30, 40, 50
Number of spray pass	1, 2, 3, 4, 5

impact velocity, coating thickness, and electrical resistance. Successful CS coating was achieved at the inlet gas pressure of \geq 0.6 MPa while no deposition was observed for $P \leq$ 0.5 MPa. Considering that there exists a critical velocity (V_{crit}) to achieve successful CS deposition on the target surface [47–50], identifying V_{crit} for Sn particle deposition on the PET surface is important to precisely define the optimal operational spraying conditions. To this end, we calculated the impact velocity of Sn particles at different inlet gas pressures in a range of $P = 0.4$ –0.7 MPa using a two-disc plate (rotary) system as shown in Fig. S2 (Supporting Information), where the spray distance is 30 mm. The details of the two-disc plate setup can be found in our previous work [51] and the Supporting Information of this study. As seen in Fig. 2a, the particles' impact velocity increases as the gas pressure rises due to the kinetic energy gain of the gas at higher pressures. The successful deposition occurs at $P \geq$ 0.6 MPa, where the average impact velocity of particles is measured at around 415 m/s. Conversely, no deposition was achieved at $P <$ 0.5 MPa, which can be explained by the insufficient kinetic energy gain of the particles for a successful bonding on the substrate surface. Instead of deposition, particles eroded the substrate surface at low pressures (\leq 0.5 MPa) (see Fig. S3a, Supporting Information).

An unstable region was also experienced for the pressure range of $0.5 < P < 0.6$ MPa, resulting in the disruptive or non-uniform coating as given in Fig. S3b, Supporting Information. In cold spraying, erosion of the target surface takes place when the particles' impact velocity is lower and also significantly higher than the V_{crit} [47]. Thus, there exists a window of deposition bounded by the critical velocity and the erosion velocity for an effective CS process [51–54]. In this regard, we calculated the particles' impact velocity as 390–515 m/s for effective CS deposition of Sn particles (5–45 μ m) on the PET surface at room temperature. The moderate impact velocities (*i.e.*, 350–390 m/s) led to unstable or disruptive coating. Below the impact velocity of 350 m/s, no deposition was observed, instead, particles eroded the substrate surface. As such, Fig. 2a provides useful information to minimize the trial-and-error processes for identifying successful CS operating pressure for Sn particle deposition on the PET polymer surface at room temperature.

As for electrical resistance and coating thickness, higher gas pressures (\geq 0.6 MPa) led to thicker coatings with lower resistance. It is likely attributed to a sufficient impact velocity of particles at higher gas pressures to achieve effective particle bonding on the target surface (see Fig. 3a). In addition, the resistance is inversely proportional to the coating thickness according to the resistance formula in Eq. (1) where ρ is the resistivity, L is the length, w is the width, and t is the thickness, which also explains the decreasing trend in the electrical resistance at higher gas pressures. Taken together, inlet gas pressure of $P = 0.7$ MPa led to the lowest resistance (*i.e.*, highest electrical conductivity) and uniform coating thickness with less standard deviation. For the following characterization studies, we selected the inlet gas pressure of $P = 0.7$ MPa owing to the prominent properties of the resultant coatings for FE at this gas pressure.

$$R = \rho \frac{L}{wt} \quad (1)$$

3.2. Effect of nozzle speed on resultant coating

Fig. 2b shows the effect of nozzle speed (NS) on resistance, thickness, and linewidth of the resultant coatings where the spray distance is constant at 30 mm. As seen in Fig. 2b, resistance tends to rise with increasing nozzle speed, which is attributed to the existence of less amount and non-uniform deposition on the target surface at higher nozzle speeds (*e.g.*, NS=150 m/s), (see Fig. S3c, Supporting Information). Conversely, the coating thickness decreases as the nozzle speed increases due to the short interaction time of the sprayed particles with the target surface, which results in less particles deposited on the surface. The cross-section SEM images in Fig. S3d (Supporting Information)

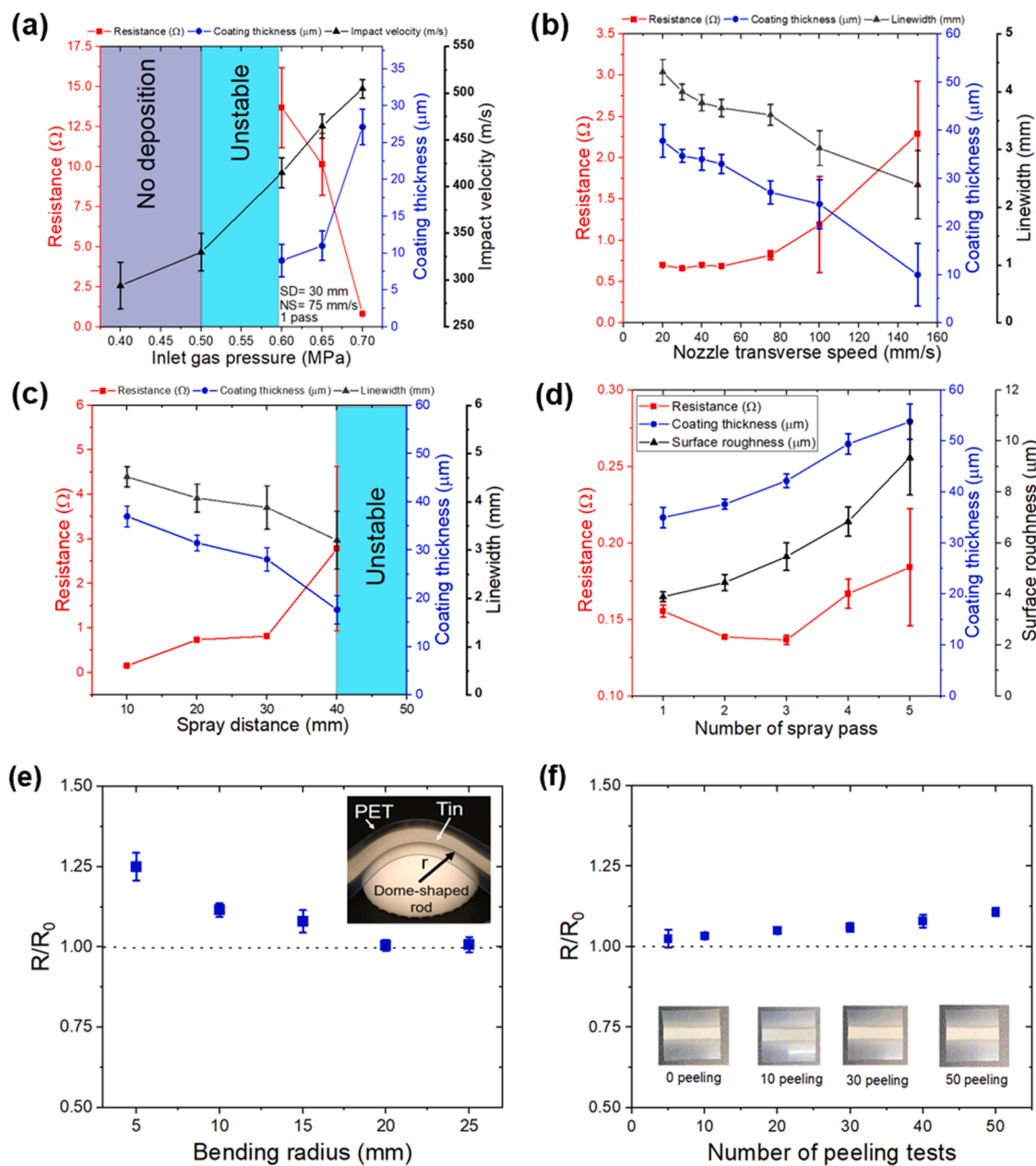


Fig. 2. Effect of (a) inlet gas pressure, (b) nozzle transverse speed, (c) spray distance, (d) the number of spray passes on electrical resistance, coating thickness, linewidth, and surface roughness; (e) The relative resistance change (R/R_0) versus different bending radius under 1000 bending cycles; (f) Resistance of the Sn coating under multiple peeling tests; (The average electrode length (L) = 30 mm and width (w) = 5 mm, where P: pressure, NS: nozzle speed, and SD: spray distance).

also correlate this trend and printing film thickness measurements at various NS. The results are comparable with the studies concluding that the coating thickness is inversely proportional to the nozzle speed [55]. It is noteworthy that electrical resistance does not critically change at the relatively lower nozzle speeds (i.e., 20–75 mm/s), whereas it sharply increases at elevated nozzle speeds (i.e., 100–150 mm/s). Possible reasons are less particle deposition as compared to lower nozzle speeds and non-uniform coating morphology throughout the CS patterning (Fig. S3c, Supporting Information). As for the line resolution, coating linewidth decreased in a quasi-linear trend with increasing NS, resulting in a smaller linewidth (2–3 mm). Although higher nozzle speeds (100–150 mm/s) led to higher resolution patterning, it resulted in less coating thickness and electrical performance with high standard deviation, which cannot be desired for FE applications where accurate and robust performance is needed.

As such, the nozzle speed should be carefully determined considering

the manufacturing and application needs where the coating uniformity, conductivity, and resolution are critical. In the present study, for the next characterizations, we selected the nozzle speed of 75 mm/s due to its moderate coating thickness, the low standard deviation in resistance and line resolution, and most importantly high-throughput manufacturing aspects and energy economics owing to relatively high-speed patterning for printed FE.

3.3. Effect of spray distance on resultant coating

The influence of spray distance (SD), also known as nozzle stand-off distance, on the coating characteristics was studied at constant pressure (0.7 MPa) and nozzle speed (75 mm/s). As seen in Fig. 2c, shorter spray distances ($SD < 30$ mm) resulted in lower electrical resistance and larger coating thickness. The lowest resistance and highest coating thickness were obtained at the spray distance of 10 mm. It is likely attributed to

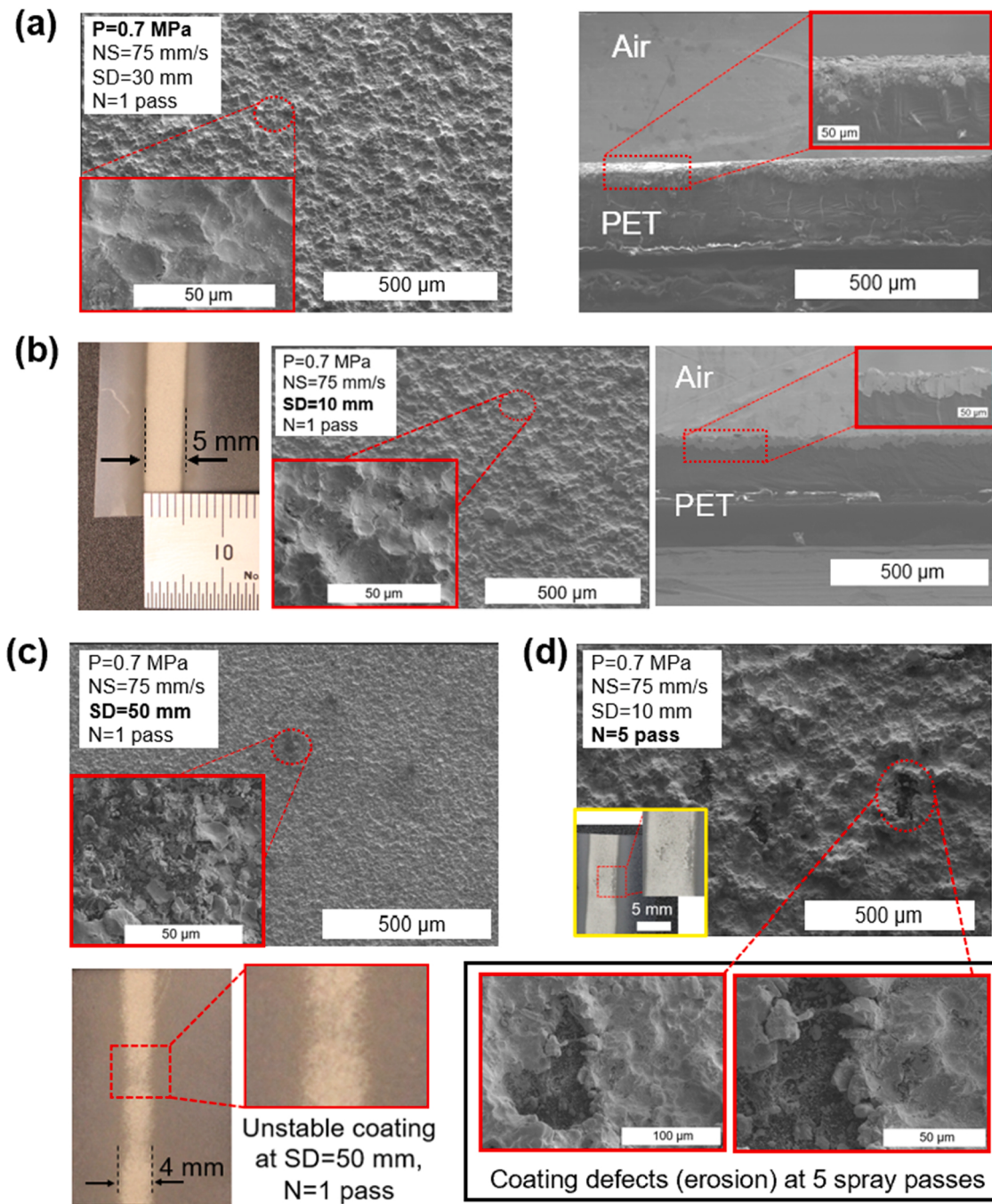


Fig. 3. Microstructures of the resultant coatings at various CS conditions; (a) $P = 0.7 \text{ MPa}$, $NS = 75 \text{ mm/s}$, $SD = 30 \text{ mm}$, $N = 1$, (b) $P = 0.7 \text{ MPa}$, $NS = 75 \text{ mm/s}$, $SD = 10 \text{ mm}$, $N = 1$, (c) $P = 0.7 \text{ MPa}$, $NS = 75 \text{ mm/s}$, $SD = 50 \text{ mm}$, $N = 1$, (d) $P = 0.7 \text{ MPa}$, $NS = 75 \text{ mm/s}$, $SD = 10 \text{ mm}$, $N = 5$.

better focusing of the spray jet onto the target surface at lower spray distances, resulting in more compact particle deposition as shown in Fig. 3b. A high standard deviation in resistance was observed at the spray distance of 40 mm due to non-uniform coating morphology. An excessive rise in spray distance beyond a threshold (*i.e.*, $> 40 \text{ mm}$) generated disruptive discontinuities on the coating surface as shown in Fig. 3c, resulting in no conductive traces on the polymer surface. As seen in Figs. S4a-b (Supporting Information), severe local porosity was observed in the coating at $SD = 50 \text{ mm}$, which would mainly be responsible for the poor conductivity. In addition, the coating discontinuities and pores can be attributed to falling gas velocity due to negative drag force at higher spray distances, which results in a significant decrease in the particles' impact velocity less than the V_{crit} [56]. Li

et al. [57] also reported that deposition efficiency (DE) of the CS process and coating thickness decrease with the increase of spray distance. We also experienced the same phenomenon, in which the particles were able to impinge on the polymer surface, but no completely continuous Sn consolidation (bonding) was achieved at $SD = 50 \text{ mm}$ (Fig. S4b, Supporting Information). The linewidth measurements in Fig. 3c also correlated with this trend having less coating thickness and linewidth at larger SD (*e.g.*, 40 mm), indicating lower DE as compared to smaller SD (*i.e.*, 10–30 mm).

Besides, the bow-shock - a shock region that inherently forms at the particles' impingement zone between the supersonic jet and the substrate- is one of the most important phenomena affecting deposition quality and efficacy in cold spraying [50,58–61]. Pattison et al. [58]

showed that there are three important regions (*i.e.*, small, medium, and large) in cold spraying as a function of spray distance (SD) that determines the deposition efficiency (DE). In detail, the shorter SD leads to a lower impact velocity due to the severe effect of the bow-shock [58]. We also experienced this phenomenon in which no successful deposition was achieved at $SD \leq 5$ mm. On the other hand, a further increase in SD more than a threshold distance significantly drops the particles' in-flight and impact velocity due to the negative drag force, resulting in low DE [57,58]. We observed a similar trend for the $SD > 40$ mm, which led to a disruptive coating on the PET polymer surface (see Fig. 3c). The results are comparable with the reported literature on the bow-shock phenomenon and stand-off distance [57,58]. Taken together, in the present study, the spray distance of 10 mm produced better focusing of the spray jet, resulting in thicker, uniform, compact, and more precise patterning on the polymer surface.

3.4. Effect of the number of spray pass on resultant coating

Fig. 2d shows the variation of resistance, thickness, and surface roughness (R_a) of the resultant coatings against the number of spray passes (N). One result is that increase in the number of spray passes led to a thicker coating due to the existence of more deposited particles on the substrate surface. Particularly, for the number of spray passes up to $N = 3$, the electrical resistance decreases as the coating thickness increases, obeying the resistance formula (*i.e.*, $R = \rho L(w.t)^{-1}$). However, for $N > 3$, the resistance began increasing with a higher standard deviation, which indicates potential erosion and/or non-uniformities formed on the coating. The microstructure of the specimen (spray pass, $N = 5$) in Fig. 3d confirms the local erosions/pores on the coating. Moreover, the surface roughness results reveal that an increase in the number of spray passes leads to higher surface roughness (R_a), thereby confirming non-uniformities with more spray passes. The results are in agreement with the study by Moridi et al. [62] whose findings reported that increasing the number of CS passes leads to mixed mode fractures in the outer layer of the coating with a high amount of pores and cracks. Also, Gillet et al. [63] showed that the 2-layer ($N = 2$) CS coating using the metal (Cu) particles in a size range of $d_{50} \approx 10\text{--}23 \mu\text{m}$ resulted in a decrease in DE from 28.7% (first layer) to 15.4% (second layer), respectively. In the present study, although a relatively thick film (*i.e.*, $\approx 40\text{--}55 \mu\text{m}$) was achieved by the spray pass of $N \geq 3$, layer-by-layer additive manufacturing of metal printings on the flexible polymers remains challenging by the CS technology, which is attributed to the bonding phenomenon of the particles. In detail, first layer deposition occurs with the impact of cold-sprayed Sn particles onto the polymer surface (*i.e.*, metal-to-polymer impact), whereas the upcoming layers should be formed on the initially metallized layer by self-bonding of Sn particles on the as-deposited metal layer. Notably, different impact velocities are needed for each layer to bond the Sn particles on the as-deposited layer to avoid potential erosion and fracture. Hence, CS operating parameters (*i.e.*, pressure, temperature, nozzle speed, nozzle distance) and also CS toolpath planning should be updated/corrected for each layer to achieve successful and relatively thicker additive manufacturing on the polymer surface.

The results suggest that CS parameters should be tailored for one single spray pass ($N = 1$) for FE applications to obtain desired electrical conductivity, coating thickness, and uniformity. As such, considering the parametric study conducted, the lowest electrical resistance (*i.e.*, 0.155Ω), uniform film thickness, and lowest surface roughness (*i.e.*, $R_a \approx 4 \mu\text{m}$) without compromising the spray resolution occurred at the optimal CS conditions of $P = 0.7 \text{ MPa}$, $NS = 75 \text{ mm/s}$, $SD = 10 \text{ mm}$, and $N = 1$. For the optimal conditions, the deposition efficiency (DE) was calculated as 14–17%. The results are comparable with the literature, in which the DE was reported as 2–30% for CS deposition of Sn and Sn mixtures (*e.g.*, Sn+Al) on the polymer surfaces (*i.e.*, CFRP, Nylon6, ABS, PEEK) at various CS conditions [38,64–67]. The relatively low DE of the CS technique on polymer surfaces is attributed to the over-spray

phenomenon. As seen in Fig. 3b and Fig. 4b, we experienced the over-spray issue at the boundary of the Sn traces. The reason is likely due to the non-linear particle velocity distribution of the impinging particles during CS. In detail, the particles at the outer cone of the spray stream have a lower velocity than the central region of the spray jet [68,69]. If the velocity of these particles is less than the critical velocity (V_{crit}), they rebound from the surface leading to erosion at the impinging boundaries instead of deposition, which further results in over-spray. It is noteworthy that although the over-spray is responsible for a relatively low DE, we did not observe a significant disruption in the CS patterning quality and electrical conductivity of the as-deposited electrodes. The as-cold sprayed Sn electrodes maintained the high-electrical conductivity without any close-circuit issue even under severe deformation conditions (see Fig. 4b).

Overall, for the optimal operation conditions, the electrical conductivity was calculated using Eq. (2), where σ is the conductivity, L is the length, R is the resistance, and S is the cross-sectional area of the coated film. For $L = 0.02 \text{ m}$, $R = 0.155 \Omega$, and $S = 1.85 \times 10^{-7} \text{ m}^2$ (*i.e.*, width ($\approx 1 \text{ mm}$) \times thickness ($37 \mu\text{m}$)), the electrical conductivity of the electrodes was calculated as $6.98 \times 10^5 \text{ S m}^{-1}$, which is only one order less than the bulk conductivity of Sn (*i.e.*, $9.17 \times 10^6 \text{ S m}^{-1}$) at room temperature. We also observed the relative resistance (R/R_0) change of the fabricated electrodes for 30 days of storage time. As seen in Fig. S5 (Supporting Information), the resistance did not increase more than 25% over a one-month storage period, indicating the long-time electrical stability of the electrodes. The resistance slightly increased along with the extension of storage, and the average resistance reached a plateau after 10 days. In addition, we tested the bending performance of the electrodes under various bending radii from 5 to 25 mm. As shown in Fig. 2e, no significant alteration in the electrical resistance appeared under 1000 bending cycles without compromising the structural integrity of the Sn layer. These mechanical tests underlined the high flexibility and conductivity of the fabricated electrodes under vigorous bending conditions.

$$\sigma = \frac{L}{RS} \quad (2)$$

3.5. Adhesion performance

The adhesion properties of the resultant coatings at optimal CS conditions were characterized using both cross-cut and Scotch tape tests according to the ASTM D3359 standard test method [70]. These qualitative tests are widely used test methods for measuring the adhesive strength of thin-film printed FE [71–73]. In this regard, first, various numbers (5–50 peelings) of Scotch tape (3 M Inc.) peeling tests were applied to the resulting CS printings, followed by measuring the R/R_0 . As shown in Fig. 2f, no significant alteration in electrical performance and intrinsic Sn coating structure was noticed after the peeling tests, which confirms the strong interfacial adhesion of the CS Sn coating. In addition, the cross-cut test based on the ASTM D3359 standard was conducted to evaluate the percent area removed given by the ASTM tape test scale [70]. Fig. S6a (Supporting Information) confirmed the high adhesion strength between the Sn coating and the PET substrate. The adhesion of Sn coating reached a 5B level according to the cross-cut tape test, having less than 5% removed area on the CS coating (Fig. S6b, Supporting Information).

Besides, after the bending tests in Fig. 2e, no noticeable difference appeared in the overall coating quality, which also confirmed the strong adhesion between the Sn layer and the substrate under bending cycles. The results are comparable and in agreement with the traditional printing approaches (*e.g.*, screen printing, ink-jet printing) in terms of adhesion strength [14,74]. As such, the resulting electrodes exhibited excellent electrical conductivity, adhesion strength, long-term stability, and flexibility. The characterization studies uncovered the process-structure-property relationships of the CS particle deposition

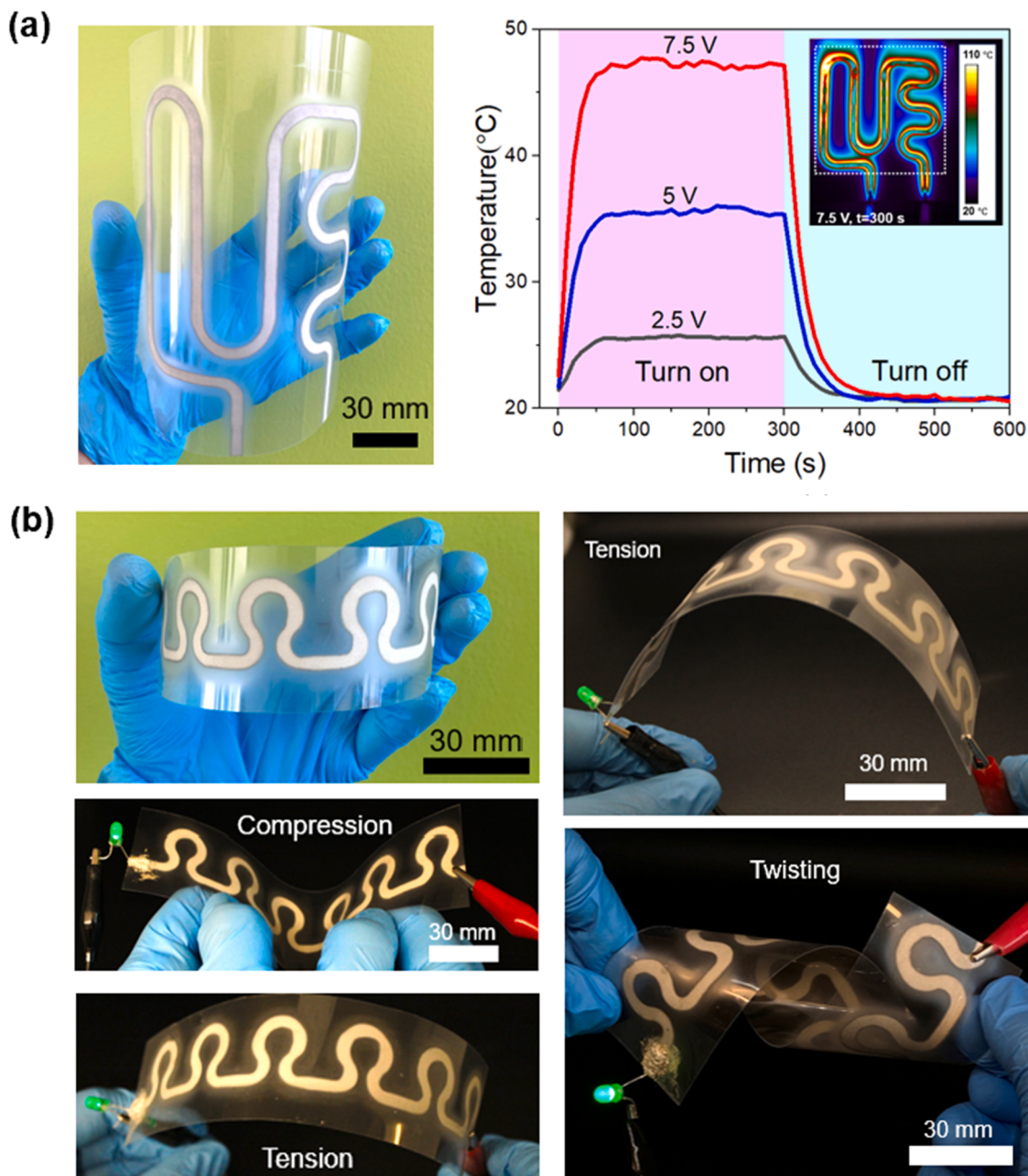


Fig. 4. Cold spray direct writing of a (a) resistive macro-heater, and (b) LED circuit and its testing under different deformation conditions.

technique for rapid production of printed FE.

3.6. Applications and prospect

To demonstrate the utility and versatility of the CS in printed flexible electronics, various CS patterning on the PET polymer sample was designed and then constructed into a macro resistive heater and a light-emitting diode (LED) circuit. Fig. 4a-b show the CS direct patterning of Sn particles on the polymer surface at the optimal CS conditions for different FE applications. A digital DC (Korad, KD6003D) power supply was used to power the resistive heater and LED circuit with alligator clips on both ends. An infrared (IR) camera (FLIR A300) was used for testing the performance of the heater. An input voltage of 2.5, 5, and 7.5 V was applied to characterize the heater. As seen in Fig. 4a (right panel) and Fig. S7 (Supporting Information), the thermal camera images confirm the applicability of the fabricated bendable resistive heater. It takes 70 s to reach maximum temperature, and then the heater cools

down to room temperature in 100 s after turning off the power. The results suggest that the fabricated flexible macro heater ($12 \times 15 \text{ cm}^2$) can be successfully used in large-area defogging applications.

A serpentine-shaped LED circuit was also fabricated to demonstrate the manufacturing capability of the CS for FE (see Fig. 4b). A green color LED light was assembled on the circuit using silver-conductive epoxy adhesive. As seen in Fig. 4b, the circuit endured vigorous tension and compression deformation without compromising the structural integrity of the functional coating. The circuit remained highly conductive under severe bending conditions, which indicates high adhesion and stability of the electrodes along a long circuit length (i.e., 180 mm). Moreover, even under the twisting deformation, no irreversible damage (e.g., crack, delamination, etc.) was observed on the circuit. The Sn printing maintained its high-electrical conductivity and structural integrity under twisting deformation without compromising high-electrical performance, indicating the robustness of the CS technique in producing FE.

In addition, considering the bonding mechanism of CS is mainly

mechanical interlocking for polymer substrates, the interlocking of the Sn particles with the PET polymer would decrease the intrinsic ductility of the polymer target. To test the ductility of the as-cold sprayed specimens, we applied continuous cyclic deformation (*i.e.*, bending, twisting) to the patterned circuit in Fig. 4b. A real-time video of the circuit under severe deformation is shown in Movie S1, Supporting Information. The as-cold sprayed polymer did not significantly compromise its intrinsic ductility, thereby indicating high flexibility. It is attributed to the strong adhesion strength of the CS printing, which led to conformal contact of the Sn electrodes with the polymer substrate.

Supplementary material related to this article can be found online at doi:10.1016/j.addma.2022.103244.

Besides, CS is promising for large-area functional metallization on flexible polymers owing to its relatively larger nozzle exit diameter. In the present study, an axisymmetric nozzle with an outlet diameter of 4.5 mm resulted in 2–5 mm resolution (linewidth) printing. On the one hand, by employing a different configuration nozzle with a larger exit aperture such as a rectangular-shaped nozzle, large-area conductive metallization on the PET surface can be achieved. In this regard, in addition to the axisymmetric nozzle, we tested a rectangular-shaped nozzle (10.35 mm × 3 mm) for Sn coating on the PET surface (Fig. S8a, Supporting Information). Without preheating the carrier-gas flow (*i.e.*, T = 25°C), no successful deposition was observed at room temperature using the rectangular-nozzle configuration. The reason is that rectangular nozzles generate stronger bow-shock due to their larger sectional area, leading to lower particle impact velocity (in our case less

than V_{crit} at room temperature) as compared to the axisymmetric nozzles [75,76]. On the other hand, preheating the carrier gas to 80 °C (see IR camera image in Fig. S8c, Supporting Information) allowed to achieve of dense and conductive Sn coating (*i.e.*, 12 mm linewidth with single-pass) on the PET surface (Fig. 8d, Supporting Information). The reason lies in: (i) increased particle velocity with higher gas temperature according to the ideal gas law (*i.e.*, Pv=RT); and (ii) thermal softening of both particles and the substrate that facilitated the particle bonding [65, 77]. The results reveal that CS technology can enable the large-area metallization of various flexible polymers, thereby having the potential to advance the rapid and high-throughput production of FE.

In addition to the abovementioned features, CS can be also potentially used for sustainable repairing of temperature-sensitive FE printed on low-thermal budget substrates (*e.g.*, PET, PEN). Conventional tin-lead soldering is not applicable for heat-sensitive substrates due to its high solder reflow temperature ($\approx 200^{\circ}\text{C}$), which is significantly higher than the glass transition temperature (T_g) of PET and PEN polymers [4]. Herein, CS could be a promising alternative to traditional tin-lead soldering for these important substrate materials owing to its low-operating temperature (*i.e.*, $< 80^{\circ}\text{C}$ along the nozzle, see IR camera image in Figs. S8b-c, Supporting Information). As example for discussion and illustration, we repaired a malfunctioned (*i.e.*, locally damaged) Sn electrode as shown in Fig. 5. In turn, the conductive Sn coating on the polymer surface was physically and chemically damaged using a plier and acetone. The localized damage was then restored by means of hand-held cold spraying owing to the portability of the low-pressure CS

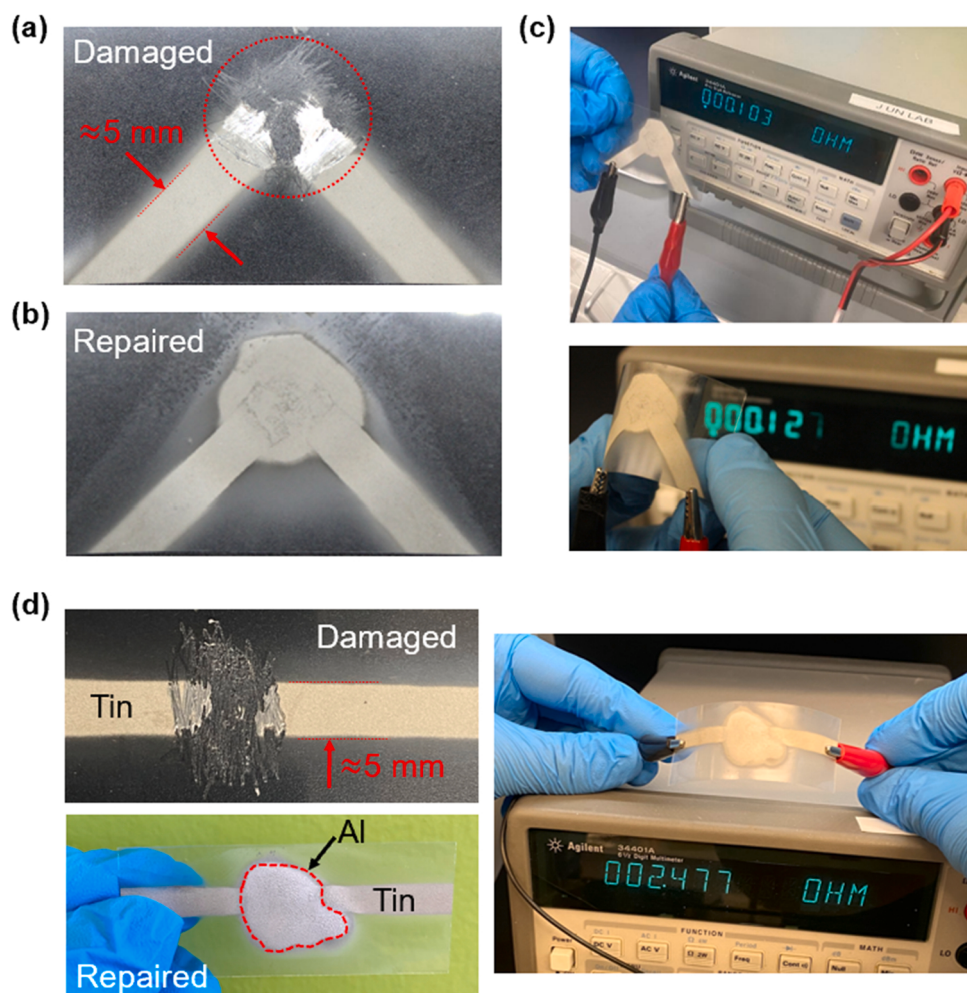


Fig. 5. (a) The damaged (malfunctioned) electrode, (b) CS-based repaired electrode, (c) electrical performance test of the restored electrode, (d) repaired Sn electrode using Al feedstock.

equipment. After CS-based repairing, as shown in Fig. 5b-c, no notable change in the intrinsic properties of both electrode and polymer substrate was observed.

We also tested the CS repair by using different feedstock materials than the electrode material. In this regard, Al powders (Centerline, Inc.) in a size range of 5–45 μm were cold sprayed onto a damaged Sn electrode. As seen in Fig. 5d, CS enabled repairing the Sn electrode through a different feedstock material such as Al. The repaired electrode maintained its functionality without significantly compromising electrical conductivity and mechanical stability. This feature of the CS technique can be also potentially utilized in the fabrication of multi-material electronics. Hereby, we mixed a number of relatively soft feedstock powders (*i.e.*, Sn + Al and Sn + Zinc) with the same weight ratio, then cold sprayed the powder mixtures onto the PET surface at low processing temperature (< 80°C). As seen in Fig. 6a-b, multi-material electrodes were successfully fabricated on a low-thermal budget flexible polymer (PET), showing the potential of CS for producing multi-material printings. The Energy Dispersive X-Ray (EDX) analyses in Fig. 6c-d also confirmed the multi-material CS coatings on the substrate surface. The clear peaks of Sn, Al, and Zn were observed on the as-cold sprayed surface (Fig. S9, Supporting Information), proving the effective multi-material coatings. Note that the existence of the Platinum (Pt) elements on the EDX images is due to the thin-layer sputtered Pt to avoid

overcharging during SEM and EDX analyses.

Considering multilayered and multi-material electronics are expected to revolutionize the field of printed electronics [78–80], this feature of CS can be valuable for multi-material and hybrid coating applications to achieve multifunctional surfaces with improved surface properties in terms of conductivity, corrosion resistance, wear resistance, bioactivity, hydrophobicity, etc. Taken together, the results suggest that CS can be effectively used for the fabrication of multi-material printings on temperature-sensitive polymers while it has the potential for repairing FE in a rapid, energy-efficient, sustainable, and eco-friendly manner against the conventional soldering techniques.

Lastly, based on the reported literature [1,3,4,81], we compared the CS particle deposition with the currently available printing methods in FE. Table 2 summarizes a comparison of the different printing techniques with printed feature properties. As seen in Table 2, CS is promising for FE in a manner that solid-state metal particles can be directly printed on flexible polymer surfaces (*e.g.*, PET) without the need of a high-temperature post-sintering or dedicated vacuum equipment. However, one of the main drawbacks of CS technology is its low spatial resolution as compared to other printing techniques. Here, it is noteworthy that the resolution of CS patterning strictly depends on the exit (outlet) dimensions of the supersonic nozzle. Employing a micronozzle, CS patterning with higher spatial resolution can be achieved. For

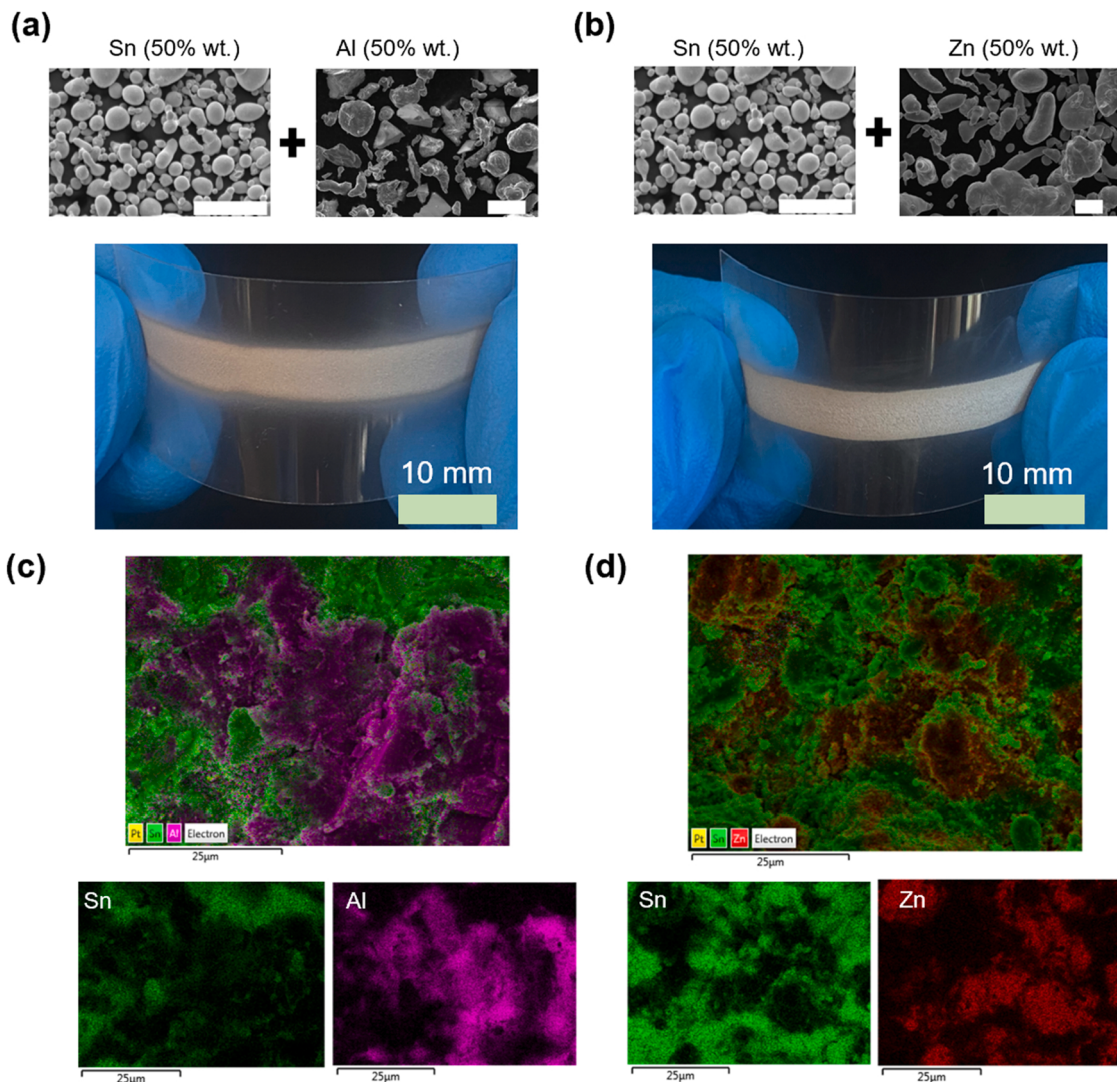


Fig. 6. Fabricated multi-material flexible electrodes: (a) Sn (50% wt.)+Al (50% wt.), (b) Sn (50% wt.)+Zn (50% wt.), (c) EDX map of the Sn + Al coating, (d) EDX map of the Sn + Zn coating; (Scale bars in SEM and EDX images= 25 μm).

Table 2

Performance comparison of various printing technologies used in flexible electronics.

Printing technologies	Resolution (linewidth)	Film thickness (μm)	Film roughness	Printing speed (m/s)	Large-area scalability	Design flexibility	Need for post-sintering
Cold spray	1–12 mm	10–55	High	0.02–0.15	Yes	High	No
Inkjet printing	30–70 μm	0.1–1	Low	0.01–0.1	Limited	High	Yes
Aerosol jet printing	50–150 μm	0.5–1	Low	0.1–1	Limited	Medium	Yes
Screen printing	50–150 μm	5–100	High	0.1–1	Yes	Low	Yes
Gravure printing	5–100 μm	0.1–1	Low	0.1–10	Yes	Low	Yes
Blade coating	200 μm	0.1–1	Low	0.01–1	Yes	Medium	Yes

instance, Sova *et.al* [82] designed a micronozzle (*i.e.*, having an outlet diameter of 1 mm), and achieved 1 mm of resolution by cold spraying Cu particles on an Al substrate using helium as the compressed gas.

In fact, it is still far beyond the spatial resolution of the other printing techniques, and remains challenging to increase the resolution of solid-state cold spraying. The reason for this is the size distribution of commercial CS powders, which is generally in a range of 5–50 μm . Although there are commercially available nanopowders (< 0.1 μm), cold spraying of these powders is difficult due to their insufficient inertia and momentum to overcome the inherent bow-shock region formed near the target surface [32,59,68]. In detail, the upon-impact trajectory of the cold-sprayed nanopowders is disrupted by the bow-shock, resulting in

no deposition on the target surface. For overcoming the bow-shock, the agglomeration process is often required to form large-enough particles before the CS process [83], but it leads to lower spatial resolution. Although CS offers high-throughput production of FE (*i.e.*, linewidth=2–12 mm, printing speed=0.15 m/s with single spray pass) at low temperatures (< 80°C), CS direct writing of high-resolution conductive traces without shadow masking remains challenging in the current situation due to the reasons stated above.

Alternatively, cold spray direct writing of Sn electrodes on the polymer surface followed by the femtosecond laser machining process could address the low-spatial resolution of the CS technique. In this regard, as illustrated in Fig. 7a, we conducted a case study on sequential

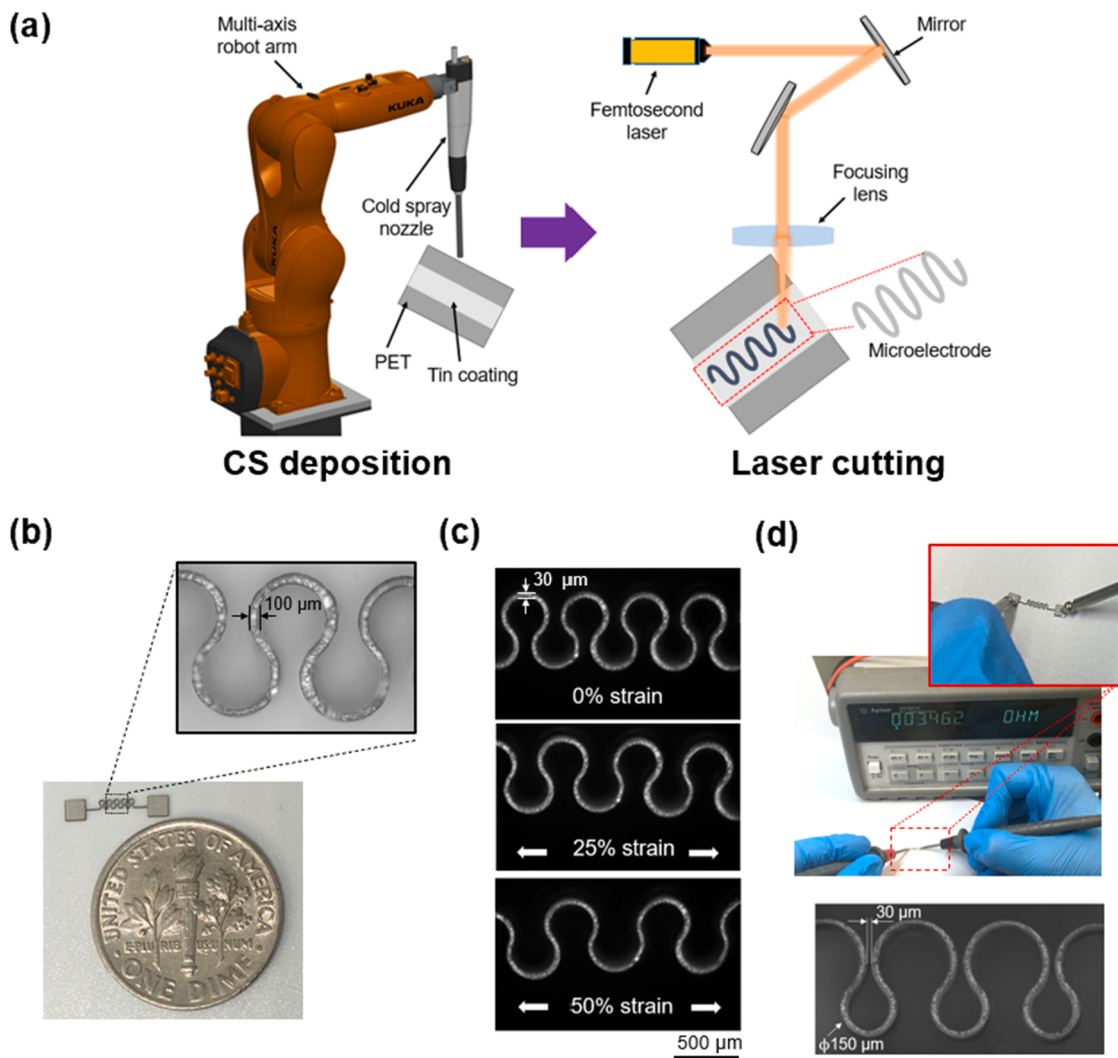


Fig. 7. (a) Schematic of the sequential CS and femtosecond laser machining approach for producing flexible and stretchable microelectrodes, (b) fabricated high-resolution electrodes, (c) electrodes (30 μm linewidth) under various stretching conditions, (d) conductivity test of the electrode with ultra-fine features (*i.e.*, 30 μm clearance).

CS and ultra-fast laser machining to achieve micron-scale printed electronics. To elaborate, first, Sn particles were directly printed on the PET surface with one-single CS pass. Then, the printed millimeter-scale Sn coating is cut out to custom-designed micron-scale electrodes by a subsequent femtosecond laser (04–1000, CARBIDE [84]) machining at the second harmonic laser wavelength (515 nm) with a pulse duration of 229 fs, a repetition rate of 2 kHz, and the pulse energy of 57 μJ , respectively. This integrated manufacturing approach enabled to fabrication of high-resolution (*i.e.*, 30–100 μm linewidth) arbitrary-shaped electrodes with ultra-fine features (see Fig. 7b), which cannot be achieved by conventional printing methods.

Moreover, owing to the manufacturing accuracy of the femtosecond laser machining, fractal-shaped electrodes can be precisely produced utilizing the proposed approach as a geometric engineering fabrication method. In detail, geometric patterning (*e.g.*, fractal design) can be applied to rigid thin films to obtain certain stretchability [85]. For that, we chose the horseshoe-shape design owing to its wide range of applications in printed electronics [86–88]. As a proof-of-the-concept, micron-scale, flexible, and stretchable electrodes were precisely achieved through the described approach (see Fig. 7b). The horseshoe-shaped electrodes with 30 μm linewidth showed up to 50% stretchability without a noticeable difference in overall Sn coating quality (see Fig. 7c). We also fabricated larger linewidth (*i.e.*, 100 μm) electrodes to show the versatility and repeatability of the described approach (Fig. S10, Supporting Information). The microelectrodes maintained conductivity and structural integrity after laser cutting without compromising intrinsic substrate and Sn coating properties (Fig. 7c-d). Moreover, ultrafine features having a 30 μm clearance (gap) between the electrodes were achieved without any sign of delamination (Fig. 7d), which can also not be obtained by the conventional printing approaches without a shadow mask.

The results of the case study suggest that sequential CS and femtosecond laser machining is a suitable approach to produce ultra-high-resolution electrodes, which can be potentially applied to various micro-sensing applications. Although the resulting microelectrodes can be used in microsensing applications, it is vital to transfer the laser-cut electrodes onto a flexible base substrate to improve the mechanical resilience of the cut-off electrodes in order to constitute compact, durable, and conformal FE. Given the above-mentioned point, future works should focus on developing a method to transfer (joint) the laser-cut electrodes onto a base flexible polymer substrate to generate resilient and high-performance micron-scale FE.

4. Conclusion

The cold spray (CS) particle deposition technique was employed and evaluated for rapid and scalable production of printed flexible electronics (FE). In this regard, micron-scale (10–45 μm) Sn particles were cold sprayed on the flexible PET polymer surface without the need for high-temperature post-sintering process that is often required by the traditional printing approaches. The effect of the CS process parameters (*i.e.*, gas pressure, nozzle speed, spray distance, number of spray pass) on resultant printings is comprehensively studied in terms of microstructure, film thickness, electrical resistance, linewidth, and surface roughness. The following conclusions can be drawn from the present work:

- CS enabled the direct writing of millimeter-scale custom-designed conductive Sn traces on the flexible PET surface in a rapid and high-throughput manner (*i.e.*, linewidth = 2–12 mm, printing speed = 0.15 m/s with single spray pass).
- The resulting electrodes exhibited excellent electrical conductivity (*i.e.*, $6.98 \times 10^5 \text{ S m}^{-1}$), flexibility, adhesion strength (5B score based on the ASTM D3359 standard), and stability by maintaining structural integrity under vigorous tension, compression, and twisting deformation.

- By leveraging the CS operational parameters, millimeter-scale FE applications such as a resistive heater and an LED circuit were fabricated to demonstrate the industrial viability of the CS for printed electronics.
- Employing a rectangular nozzle with an exit aperture of 10.35 mm \times 3 mm, large-area functional metallization (*i.e.*, linewidth = 12 mm for a single pass) was achieved, which also proved the large-scale processing compatibility of CS for FE.
- CS, owing to its low operating temperature, was utilized for sustainable repairing of low-thermal budget FE without compromising the intrinsic substrate and coating properties, thereby CS has the potential to address the ever-increasing number of global electronic waste.
- Multi-material (Sn+Al and Sn+Zinc) deposition experiments demonstrated the feasibility of the CS technique for the fabrication of multi-material hybrid electronics.
- Although CS has lower spatial resolution than conventional printing methods, arbitrarily designed (*e.g.*, horseshoe-shaped) ultra-high resolution (*i.e.*, 30 μm linewidth) flexible and stretchable electrodes were fabricated by coupling CS with a subsequent femtosecond laser machining process, which also proved the scalability of the CS technique in FE.
- Overall, the results of this study revealed the underlying performance of CS in printed electronics by providing a guideline for rapid and scalable production of FE.

As for future works, the authors will focus on developing a method to transfer (joint) the laser-cut micron-scale electrodes onto a base flexible polymer substrate to increase the mechanical resilience of the electrodes for producing high-performance micron-scale FE. We envision that CS-based printing will be a promising approach for direct and scalable writing (from macro to micro), and sustainable repairing of flexible electronics in the future.

CRediT authorship contribution statement

Semih Akin: Writing – original draft, Visualization, Methodology, Investigation, Formal analysis, Data curation, Conceptualization. **Seungjun Lee:** Validation, Methodology, Investigation, experiments, characterization. **Seunghwan Jo:** Validation, Methodology, Investigation, experiments, characterization. **Duygu G. Ruzgar:** Validation, Investigation, Experiments, characterization. **Karthick Subramanian:** Validation, Investigation, Experiments. **Jung T. Tsai:** Validation, Experiments. **Martin B.G. Jun:** Writing – review & editing, Supervision, Resources, Methodology, Conceptualization.

Declaration of Competing Interest

The authors declare that they have no known competing financial interests or personal relationships that could have appeared to influence the work reported in this paper.

Data Availability

Data will be made available on request.

Acknowledgements

The first author of this study, S.A, acknowledges a scholarship through the Office of Overseas Scholarship Programs from the Republic of Turkey Ministry of National Education. S.A also acknowledges a fellowship (Lambert Fellowship) support from Purdue University, School of Mechanical Engineering. S.L acknowledges a scholarship support by Institute of Information & Communications Technology Planning & Evaluation (IITP) grant funded by the Korea Government (MSIT) (No.2021-0-01577). D.G.R acknowledges a fellowship (2219-

International Postdoctoral Fellowship Program) by the Scientific and Technological Research Council of Turkey (TUBITAK). K.S acknowledges DST, Government of India for the SERB Purdue University OVDF project grant (No. SB/S9/Z-03/2017-X (2019–20)).

Appendix A. Supporting information

Supplementary data associated with this article can be found in the online version at [doi:10.1016/j.addma.2022.103244](https://doi.org/10.1016/j.addma.2022.103244).

References

- [1] Q. Huang, Y. Zhu, Printing conductive nanomaterials for flexible and stretchable electronics: a review of materials, processes, and applications, *Adv. Mater. Technol.* 4 (2019) 1–41, <https://doi.org/10.1002/admt.201800546>.
- [2] Y. Bonnassieux, C.J. Brabec, Y. Cao, T.B. Carmichael, M.L. Chabiny, K.T. Cheng, G. Cho, A. Chung, C.L. Cobb, A. Distler, H.J. Egelhaaf, G. Grau, X. Guo, G. Haghishianian, T.C. Huang, M.M. Hussain, B. Iniguez, T.M. Lee, L. Li, Y. Ma, D. Ma, M.C. McAlpine, T.N. Ng, R. Österbacka, S.N. Patel, J. Peng, H. Peng, J. Rivnay, L. Shao, D. Steinbart, R.A. Street, V. Subramanian, L. Torsi, Y. Wu, The 2021 flexible and printed electronics roadmap, *Flex. Print. Electron.* 6 (2021), 023001, <https://doi.org/10.1088/2058-8585/abf986>.
- [3] J. Wiklund, A. Karakoç, T. Palko, H. Yigitler, K. Ruttki, R. Jäntti, J. Paltakari, A review on printed electronics: fabrication methods, inks, substrates, applications and environmental impacts, *J. Manuf. Mater. Process.* 5 (2021) 89, <https://doi.org/10.3390/jmmp5030089>.
- [4] Y. Khan, A. Thielens, S. Muin, J. Ting, C. Baumbauer, A.C. Arias, A new frontier of printed electronics: flexible hybrid electronics, *Adv. Mater.* 32 (2020), 1905279, <https://doi.org/10.1002/adma.201905279>.
- [5] M.G. Mohammed, R. Kramer, All-printed flexible and stretchable electronics, *Adv. Mater.* 29 (2017), 1604965, <https://doi.org/10.1002/adma.201604965>.
- [6] S. Lee, Q. Shi, C. Lee, From flexible electronics technology in the era of IoT and artificial intelligence toward future implanted body sensor networks, *APL Mater.* 7 (2019), 031302, <https://doi.org/10.1063/1.5063498>.
- [7] T. Han, A. Nag, N. Afsharmanesh, S.C. Mukhopadhyay, S. Kundu, Y. Xu, Laser-Assisted printed flexible sensors: a review, *Sensors* 19 (2019) 1462, <https://doi.org/10.3390/s19061462>.
- [8] G.L. Goh, M.F. Tay, J.M. Lee, J.S. Ho, L.N. Sim, W.Y. Yeong, T.H. Chong, Potential of printed electrodes for electrochemical impedance spectroscopy (EIS): toward membrane fouling detection, *Adv. Electron. Mater.* 7 (2021), 2100043, <https://doi.org/10.1002/AELM.202100043>.
- [9] T. Chang, S. Akin, M.K. Kim, L. Murray, B. Kim, S. Cho, S. Hur, S. Teke, L. Couetil, M.B. Jun, C.H. Lee, Programmable dual regime spray for large-scale and custom-designed electronic textiles, *Adv. Mater.* (2021), 2108021, <https://doi.org/10.1002/adma.202108021>.
- [10] D.J. Roach, C. Roberts, J. Wong, X. Kuang, J. Kovitz, Q. Zhang, T.G. Spence, H. J. Qi, Surface modification of fused filament fabrication (FFF) 3D printed substrates by inkjet printing polyimide for printed electronics, *Addit. Manuf.* 36 (2020), 101544, <https://doi.org/10.1016/j.addma.2020.101544>.
- [11] D. Maddipatla, B.B. Narakathu, M. Atashbar, Recent progress in manufacturing techniques of printed and flexible sensors: a review, *Biosensors* 10 (2020) 199, <https://doi.org/10.3390/bios10120199>.
- [12] Q. Li, J. Zhang, Q. Li, G. Li, X. Tian, Z. Luo, F. Qiao, X. Wu, J. Zhang, Review of printed electrodes for flexible devices, *Front. Mater.* 5 (2019) 77, <https://doi.org/10.3389/fmats.2018.00077>.
- [13] L. Nayak, S. Mohanty, S. Kumar Nayak, A. Ramadoss, A review on inkjet printing of nanoparticle inks for flexible electronics, *J. Mater. Chem. C* 7 (2019) 8771, <https://doi.org/10.1039/c9tc01630a>.
- [14] P. He, J. Cao, H. Ding, C. Liu, J. Neilson, Z. Li, I.A. Kinloch, B. Derby, Screen-printing of a highly conductive graphene ink for flexible printed electronics, *ACS Appl. Mater. Interfaces* 11 (2019) 32225–32234, <https://doi.org/10.1021/acsmami.9b04589>.
- [15] E.B. Secor, S. Lim, H. Zhang, C.D. Frisbie, L.F. Francis, M.C. Hersam, Gravure printing of graphene for large-area flexible electronics, *Adv. Mater.* 26 (2014) 4533–4538, <https://doi.org/10.1002/ADMA.201401052>.
- [16] J. Zhu, D. Han, X. Wu, J. Ting, S. Du, A.C. Arias, Highly flexible transparent micromesh electrodes via blade-coated polymer networks for organic light-emitting diodes, *ACS Appl. Mater. Interfaces* 12 (2020) 31687–31695, https://doi.org/10.1021/ACSMI.0C07299/SUPPL_FILE/AM0C07299_SI_001.PDF.
- [17] N.J. Wilkinson, M.A.A. Smith, R.W. Kay, R.A. Harris, A review of aerosol jet printing—a non-traditional hybrid process for micro-manufacturing, *Int. J. Adv. Manuf. Technol.* 105 (2019) 4599–4619, <https://doi.org/10.1007/s00170-019-03438-2>.
- [18] A.D. Valentine, T.A. Busbee, J.W. Boley, J.R. Raney, A. Chortos, A. Kotikian, J. D. Berrigan, M.F. Durstock, J.A. Lewis, Hybrid 3D printing of soft electronics, *Adv. Mater.* 29 (2017), 1703817, <https://doi.org/10.1002/adma.201703817>.
- [19] K. Suganuma, Introduction to Printed Electronics, Springer, New York, New York, NY, 2014, <https://doi.org/10.1007/978-1-4614-9625-0>.
- [20] S. Yin, P. Cavaliere, B. Aldwell, R. Jenkins, H. Liao, W. Li, R. Lupoi, Cold spray additive manufacturing and repair: fundamentals and applications, *Addit. Manuf.* 21 (2018) 628–650, <https://doi.org/10.1016/j.addma.2018.04.017>.
- [21] R.N. Raoelison, Y. Xie, T. Sapanathan, M.P. Planche, R. Kromer, S. Costil, C. Langlade, Cold gas dynamic spray technology: A comprehensive review of processing conditions for various technological developments till to date, *Addit. Manuf.* 19 (2018) 134–159, <https://doi.org/10.1016/j.addma.2017.07.001>.
- [22] S. An, B. Joshi, A.L. Yarin, M.T. Swihart, S.S. Yoon, Supersonic cold spraying for energy and environmental applications: one-step scalable coating technology for advanced micro- and nanotextured materials, *Adv. Mater.* 32 (2020), 1905028, <https://doi.org/10.1002/adma.201905028>.
- [23] R. Della Gatta, A. Viscusi, A.S. Perna, A. Caraviello, A. Astarita, Feasibility of steel powder deposition on composites through cold spray, *Mater. Manuf. Process.* 36 (2021) 281–291, <https://doi.org/10.1080/10426914.2020.1832693>.
- [24] A. Viscusi, Numerical investigations on the rebound phenomena and the bonding mechanisms in cold spray processes, in: AIP Conf. Proc., AIP Publishing LLC AIP Publishing, 2018, <https://doi.org/10.1063/1.5034957>.
- [25] A. Viscusi, A. Astarita, L. Carrino, G. D'Avino, C. de Nicola, P.L. Maffettone, G. P. Reina, S. Russo, A. Squillace, Experimental study and numerical investigation of the phenomena occurring during long duration cold spray deposition, *Int. Rev. Model. Simul.* 11 (2018) 84–92, <https://doi.org/10.15866/iremos.v11i2.13619>.
- [26] A. Viscusi, A. Astarita, S. Genna, C. Leone, On the influence of different superficial laser texturing on the deposition of powders through cold spray process, *Trans. Inst. Met. Finish.* 96 (2018) 34–40, <https://doi.org/10.1080/00202967.2018.1403096>.
- [27] A. Papyrin, V. Kosarev, S. Klinkov, A. Alkhimov, V.M. Fomin, Cold Spray Technology, Elsevier Ltd., 2007, <https://doi.org/10.1016/B978-0-08-045155-8.X5000-5>.
- [28] Z.-S. Wang, K. Sayama, H. Sugihara, Efficient Eosin Y Dye-Sensitized Solar Cell Containing Br-/Br-3-Electrolyte, 2005. (<https://doi.org/10.1021/jp053260h>).
- [29] S. An, B. Joshi, A.L. Yarin, M.T. Swihart, S.S. Yoon, Supersonic cold spraying for energy and environmental applications: one-step scalable coating technology for advanced micro- and nanotextured materials, *Adv. Mater.* 32 (2020), 1905028, <https://doi.org/10.1002/adma.201905028>.
- [30] A.S. Perna, A. Astarita, P. Carbone, X. Guthmann, A. Viscusi, Characterization of cold-spray coatings on fiber-reinforced polymers through nanoindentation tests, 11 (2021) 331, *Met* 11 (2021) 331, <https://doi.org/10.3390/MET11020331>.
- [31] S. Zhou, C.A. Bernard, K. Ravi, H. Saito, Y. Ichikawa, K. Ogawa, S. Yin, Development and characterization of photocatalytic GaN coatings by cold spray process, *J. Therm. Spray. Technol.* 30 (2021) 1294–1309, <https://doi.org/10.1007/s11666-021-01207-w>.
- [32] V. Champagne, D. Helfritch, The unique abilities of cold spray deposition, *Int. Mater. Rev.* 61 (2016) 437–455, <https://doi.org/10.1080/09506608.2016.1194948>.
- [33] J.-G. Lee, D.-Y. Kim, T.-G. Kim, J.-H. Lee, S.S. Al-Deyab, H.W. Lee, J.S. Kim, D. H. Yang, A.L. Yarin, S.S. Yoon, Supersonically sprayed copper-nickel microparticles as flexible and printable thin-film high-temperature heaters, *Adv. Mater. Interfaces* 4 (2017), 1700075, <https://doi.org/10.1002/admi.201700075>.
- [34] S. Bhattacharya, A. Lutfurakhman, J.M. Hoey, O.F. Swenson, R. Sailer, Micro cold spray direct write process, *ASME Int. Mech. Eng. Congr. Expo. Proc.* 7 (2013) 907–911, <https://doi.org/10.1115/IMECE2012-86601>.
- [35] H.S. Jo, S. An, C.W. Park, D.Y. Woo, A.L. Yarin, S.S. Yoon, Wearable, stretchable, transpniwires all-in-one soft sensor formed from supersonically sprayed silver nanowires, *ACS Appl. Mater. Interfaces* 11 (2019) 40232–40242, <https://doi.org/10.1021/acsami.9b12847>.
- [36] E. Samuel, T.-G. Kim, C.-W. Park, B. Joshi, M.T. Swihart, S.S. Yoon, Supersonically Sprayed Zn 2 SnO 4 /SnO 2 /CNT Nanocomposites for High-Performance Supercapacitor Electrodes, 2019. (<https://doi.org/10.1021/acssuschemeng.9b02549>).
- [37] J.G. Lee, D.Y. Kim, J.H. Lee, M.W. Kim, S. An, H.S. Jo, C. Nervi, S.S. Al-Deyab, M. T. Swihart, S.S. Yoon, Scalable binder-free supersonic cold spraying of nanotextured cupric oxide (CuO) films as efficient photocathodes, *ACS Appl. Mater. Interfaces* 8 (2016) 15406–15414, <https://doi.org/10.1021/acsmami.6b03968>.
- [38] A.C. Liberati, H. Che, P. Vo, S. Yue, Observation of an indirect deposition effect while cold spraying Sn-Al mixed powders onto carbon fiber reinforced polymers, *J. Therm. Spray. Technol.* 29 (2020) 134–146, <https://doi.org/10.1007/s11666-019-00967-w>.
- [39] M. Winnicki, A. Baszcuzk, M. Rutkowska-Gorczyca, A. Malachowska, A. Ambroziak, Corrosion resistance of tin coatings deposited by cold spraying, [Http://Dx.Doi.Org/10.1080/02670844.2016.1190064](http://Dx.Doi.Org/10.1080/02670844.2016.1190064) 32 (2016) 691–700, <https://doi.org/10.1080/02670844.2016.1190064>.
- [40] Y.W. Kim, S. Akin, H. Yun, S. Xu, W. Wu, M. Byung, G. Jun, Enhanced performance of triboelectric nanogenerators and sensors via cold spray particle deposition, *ACS Appl. Mater. Interfaces* (2022), <https://doi.org/10.1021/ACSMI.2C09367>.
- [41] H. Che, A.C. Liberati, X. Chu, M. Chen, A. Nobari, P. Vo, S. Yue, Metallization of polymers by cold spraying with low melting point powders, *Surf. Coat. Technol.* 418 (2021), 127229, <https://doi.org/10.1016/j.surfcoat.2021.127229>.
- [42] A.C. Liberati, H. Che, P. Fallah, P. Vo, S. Yue, Pull-off testing and electrical conductivity of sn-based metal powder mixtures cold sprayed on carbon fiber-reinforced polymers, *J. Therm. Spray. Technol.* (2022) 1–21, <https://doi.org/10.1007/s11666-022-01405-0>.
- [43] R. Melentiev, N. Yu, G. Lubineau, Polymer metallization via cold spray additive manufacturing: a review of process control, coating qualities, and prospective applications, *Addit. Manuf.* 48 (2021), 102459, <https://doi.org/10.1016/j.addma.2021.102459>.
- [44] S. Akin, J.-T. Tsai, M.S. Park, Y.H. Jeong, M. Jun, Fabrication of electrically conductive patterns on ABS polymer using low-pressure cold spray and electroless plating, *J. Micro Nano-Manuf.* 8 (2021), <https://doi.org/10.1115/1.4049578>.

- [45] J.-T. Tsai, S. Akin, F. Zhou, M.S. Park, D.F. Bahr, M.B.-G. Jun, Electrically conductive metallized polymers by cold spray and co-electroless deposition, *ASME Open J. Eng.* 1 (2022), <https://doi.org/10.1115/1.4053781>.
- [46] Silver powder, 2–3.5um, 99.9+ trace metals 7440–22-4, (n.d.). (<https://www.sigmapractical.com/US/en/product/aldrich/327085>) (Accessed 13 June 2022).
- [47] M. Kamaraj, V.M. Radhakrishnan, Cold spray coating diagram: bonding properties and construction methodology, *J. Therm. Spray. Technol.* 28 (2019) 756–768, <https://doi.org/10.1007/s11666-019-00853-5>.
- [48] T. Schmidt, F. Gärtner, H. Assadi, H. Kreye, Development of a generalized parameter window for cold spray deposition, *Acta Mater.* 54 (2006) 729–742, <https://doi.org/10.1016/j.actamat.2005.10.005>.
- [49] S. Grigoriev, A. Okunkova, A. Sova, P. Bertrand, I. Smurov, Cold spraying: from process fundamentals towards advanced applications, *Surf. Coat. Technol.* 268 (2015) 77–84, <https://doi.org/10.1016/j.surfcoat.2014.09.060>.
- [50] H. Assadi, H. Kreye, F. Gärtner, T. Klassen, Cold spraying – a materials perspective, *Acta Mater.* 116 (2016) 382–407, <https://doi.org/10.1016/j.actamat.2016.06.034>.
- [51] J.-T. Tsai, S. Akin, F. Zhou, D.F. Bahr, M.B.-G. Jun, Establishing a cold spray particle deposition window on polymer substrate, *J. Therm. Spray. Technol.* (2021) 1–12, <https://doi.org/10.1007/s11666-021-01179-x>.
- [52] T. Schmidt, F. Gärtner, H. Assadi, H. Kreye, Development of a generalized parameter window for cold spray deposition, *Acta Mater.* 54 (2006) 729–742, <https://doi.org/10.1016/j.actamat.2005.10.005>.
- [53] T. Schmidt, H. Assadi, F. Gärtner, H. Richter, T. Stoltenhoff, H. Kreye, T. Klassen, From particle acceleration to impact and bonding in cold spraying, *J. Therm. Spray. Technol.* 18 (2009) 794–808, <https://doi.org/10.1007/s11666-009-9357-7>.
- [54] M. Hassani-Gangaraj, D. Veysset, K.A. Nelson, C.A. Schuh, Melt-driven erosion in microparticle impact, *Nat. Commun.* 9 (2018) 1–7, <https://doi.org/10.1038/s41467-018-07509-y>.
- [55] H. Wu, X. Xie, M. Liu, C. Chen, H. Liao, Y. Zhang, S. Deng, A new approach to simulate coating thickness in cold spray, *Surf. Coat. Technol.* 382 (2020), 125151, <https://doi.org/10.1016/j.surfcoat.2019.125151>.
- [56] J. Pattison, S. Celotto, A. Khan, W. O'Neill, Standoff distance and bow shock phenomena in the Cold Spray process, *Surf. Coat. Technol.* 202 (2008) 1443–1454, <https://doi.org/10.1016/j.surfcoat.2007.06.065>.
- [57] W.Y. Li, C. Zhang, X.P. Guo, G. Zhang, H.L. Liao, C.J. Li, C. Coddet, Effect of standoff distance on coating deposition characteristics in cold spraying, *Mater. Des.* 29 (2008) 297–304, <https://doi.org/10.1016/j.matdes.2007.02.005>.
- [58] J. Pattison, S. Celotto, A. Khan, W. O'Neill, Standoff distance and bow shock phenomena in the Cold Spray process, *Surf. Coat. Technol.* 202 (2008) 1443–1454, <https://doi.org/10.1016/j.surfcoat.2007.06.065>.
- [59] T.C. Jen, L. Li, W. Cui, Q. Chen, X. Zhang, Numerical investigations on cold gas dynamic spray process with nano- and microsize particles, *Int. J. Heat Mass Transf.* 48 (2005) 4384–4396, <https://doi.org/10.1016/j.ijheatmasstransfer.2005.05.008>.
- [60] S. Garmeh, M. Jadidi, A. Dolatabadi, Three-dimensional modeling of cold spray for additive manufacturing, *J. Therm. Spray. Technol.* 29 (2020) 38–50, <https://doi.org/10.1007/s11666-019-00928-3>.
- [61] S. Yin, X.F. Wang, W.Y. Li, B.P. Xu, Numerical study on the effect of substrate angle on particle impact velocity and normal velocity component in cold gas dynamic spraying based on CFD, *J. Therm. Spray. Technol.* 19 (2010) 1155–1162, <https://doi.org/10.1007/s11666-010-9510-3>.
- [62] A. Moridi, S.M. Hassani Gangaraj, S. Vezzu, M. Guagliano, Number of passes and thickness effect on mechanical characteristics of cold spray coating, *Procedia Eng.* 74 (2014) 449–459, <https://doi.org/10.1016/J.PROENG.2014.06.296>.
- [63] V. Gillet, E. Aubignat, S. Costil, B. Courant, C. Langlade, P. Casari, W. Knapp, M. P. Planche, Development of low pressure cold sprayed copper coatings on carbon fiber reinforced polymer (CFRP), *Surf. Coat. Technol.* 364 (2019) 306–316, <https://doi.org/10.1016/j.surfcoat.2019.01.011>.
- [64] A. Matachowska, M. Winnicki, T. Konat, L. Piwowarczyk, A. Pawłowski, M. Stachowicz Ambroziak, Possibility of spraying of copper coatings on polyamide 6 with low pressure cold spray method, *Surf. Coat. Technol.* 318 (2017) 82–89, <https://doi.org/10.1016/J.SURFCOAT.2017.02.001>.
- [65] H. Che, P. Vo, S. Yue, Metallization of carbon fibre reinforced polymers by cold spray, *Surf. Coat. Technol.* 313 (2017) 236–247, <https://doi.org/10.1016/j.surfcoat.2017.01.083>.
- [66] H. Che, A. Liberati, P. Vo, S. Yue, Cold spray of mixed Sn-Zn and Sn-Al powders on carbon fiber reinforced polymers, *Mater. Sci. Forum* 941 (2018) 1892–1897, <https://doi.org/10.4028/WWW.SCIENTIFIC.NET/MSF.941.1892>.
- [67] H. Che, X. Chu, P. Vo, S. Yue, Metallization of various polymers by cold spray, *J. Therm. Spray. Technol.* 27 (2018) 169–178, <https://doi.org/10.1007/s11666-017-0663-1>.
- [68] S. Akin, P. Wu, J.-T. Tsai, C. Nath, J. Chen, M.B.-G. Jun, A study on droplets dispersion and deposition characteristics under supersonic spray flow for nanomaterial coating applications, *Surf. Coat. Technol.* 426 (2021), 127788, <https://doi.org/10.1016/j.surfcoat.2021.127788>.
- [69] S. Yin, Q. Liu, H. Liao, X. Wang, Effect of injection pressure on particle acceleration, dispersion and position in cold spray, *Comput. Mater. Sci.* 90 (2014) 7–15, <https://doi.org/10.1016/j.commatsci.2014.03.055>.
- [70] ASTM D3359, ASTM D3359: Measuring Adhesion by Tape Test, Standard Test Methods for, 2009. (<https://www.astm.org/DATABASE.CART/HISTORICAL/D3359-02.htm>) (Accessed 20 October 2021).
- [71] A. Zareei, S. Gopalakrishnan, Z. Mutlu, Z. He, S. Peana, H. Wang, R. Rahimi, Highly conductive copper-silver bimodal paste for low-cost printed electronics, *ACS Appl. Electron. Mater.* 3 (2021) 3352–3364, <https://doi.org/10.1021/acsaelm.1c00345>.
- [72] R. Van Dommelen, R.I. Haque, O. Chandran, S. Lani, D. Briand, In-situ laser sintering for the fabrication of fully 3D printed electronics composed of elastomeric materials, *Flex. Print. Electron.* 6 (2021), 045003, <https://doi.org/10.1088/2058-8585/AC20C0>.
- [73] S. Akin, T. Gabor, S. Jo, H. Joe, J.T. Tsai, Y. Park, C.H. Lee, M.S. Park, M.B.G. Jun, Dual regime spray deposition based laser direct writing of metal patterns on polymer substrates, *J. Micro Nano-Manuf.* 8 (2020), <https://doi.org/10.1115/1.4046282>.
- [74] M.A. Riheen, T.K. Saha, P.K. Sekhar, Inkjet Printing on PET Substrate, *J. Electrochem. Soc.* 166 (2019) B3036–B3039, <https://doi.org/10.1149/2.0091909JES/XML>.
- [75] S. Yin, X.Fang Wang, W.Ya Li, Computational analysis of the effect of nozzle cross-section shape on gas flow and particle acceleration in cold spraying, *Surf. Coat. Technol.* 205 (2011) 2970–2977, <https://doi.org/10.1016/j.surfcoat.2010.11.002>.
- [76] T. Gabor, S. Akin, J.-T. Tsai, S. Jo, F. Al-Najjar, M.B.-G. Jun, Numerical Studies on Cold Spray Particle Deposition Using a Rectangular Nozzle, Vol. 1 Addit. Manuf. Biomanufacturing; Life Cycle Eng. Manuf. Equip. Autom. Nano/Micro/Meso Manuf., 2022. (<https://doi.org/10.1115/MSEC2022-85673>).
- [77] H. Assadi, F. Gärtner, T. Stoltenhoff, H. Kreye, Bonding mechanism in cold gas spraying, *Acta Mater.* 51 (2003) 4379–4394, [https://doi.org/10.1016/S1359-6454\(03\)00274-X](https://doi.org/10.1016/S1359-6454(03)00274-X).
- [78] G.L. Goh, H. Zhang, T.H. Chong, W.Y. Yeong, 3D printing of multilayered and multifaterial electronics: a review, *Adv. Electron. Mater.* 7 (2021), 2100445, <https://doi.org/10.1002/AELM.202100445>.
- [79] D. Lehmhus, M. Busse, A. Von Hehl, E. Jägle, State of the Art and Emerging Trends in Additive Manufacturing: From Multi-Material processes to 3D printed Electronics, (n.d.). (<https://doi.org/10.1051/matecconf/201818803013>).
- [80] B. Lu, H. Lan, H. Liu, B. Lu, H. Lan, H. Liu, Additive manufacturing frontier: 3D printing electronics, *Opto-Electron. Adv.* 1 (2018), <https://doi.org/10.29026/OEA.2018.170004> (170004–170004).
- [81] K. Suganuma, Printing Technology, in: Springer, New York, NY, 2014, pp. 23–48, https://doi.org/10.1007/978-1-4614-9625-0_2.
- [82] A. Sova, S. Klinkov, V. Kosarev, N. Ryashin, I. Smurov, Preliminary study on deposition of aluminium and copper powders by cold spray micronozzle using helium, *Surf. Coat. Technol.* 220 (2013) 98–101, <https://doi.org/10.1016/j.surfcoat.2012.09.036>.
- [83] W. Li, H. Assadi, F. Gaertner, S. Yin, A review of advanced composite and nanostructured coatings by solid-state cold spraying process, *Crit. Rev. Solid State Mater. Sci.* 44 (2019) 109–156, <https://doi.org/10.1080/10408436.2017.1410778>.
- [84] S. Jo, S. Akin, M.S. Park, M.B.G. Jun, Selective metallization on glass surface by laser direct writing combined with supersonic particle deposition, *Manuf. Lett.* 31 (2022) 64–68, <https://doi.org/10.1016/j.mfglet.2021.07.009>.
- [85] Y. Xiao, M. Wang, Y. Li, Z. Sun, Z. Liu, L. He, R. Liu, High-adhesive flexible electrodes and their manufacture: a review, *Micromachines* 12 (2021) 1505, <https://doi.org/10.3390/mi12121505>.
- [86] J.A. Fan, W.H. Yeo, Y. Su, Y. Hattori, W. Lee, S.Y. Jung, Y. Zhang, Z. Liu, H. Cheng, L. Falgout, M. Bajema, T. Coleman, D. Gregoire, R.J. Larsen, Y. Huang, J.A. Rogers, Fractal design concepts for stretchable electronics, *Nat. Commun.* 5 (2014), <https://doi.org/10.1038/ncomms4266>.
- [87] N. Qaiser, A.N. Damdam, S.M. Khan, S. Bunaiyan, M.M. Hussain, Design criteria for horseshoe and spiral-based interconnects for highly stretchable electronic devices, *Adv. Funct. Mater.* 31 (2021), 2007445, <https://doi.org/10.1002/adfm.202007445>.
- [88] M. Gonzalez, F. Axisa, M. Vanden Bulcke, D. Brosteaux, B. Vandervelde, J. Vanfleteren, Design of metal interconnects for stretchable electronic circuits, *Microelectron. Reliab.* 48 (2008) 825–832, <https://doi.org/10.1016/j.microrel.2008.03.025>.